Computer Assisted Mechanics & Engineering Sciences, 1: 49–75, 1994.

Flow approach — finite element model for stamping processes versus experiment

Włodzimierz Sosnowski
Institute of Fundamental Technological Research, Polish Academy of Sciences, Warsaw, Poland

(Received January 10, 1994)

In this paper, information on a sheet metal formig simulation program based on flow approach is provided and comparisons between numerical and experimental results are presented. Elastic spring-back effects and residual stresses are predicted by means of a large-strain elasto-viscoplastic finite element model recently proposed for this class of problems involving large deformations and changes in geometry.

A wide experimental program performed in a sheet stamping factory is shortly described. Tests included the deep drawing of circular and rectangular blanks with cylindrical and prismatic tools, respectively. Different die and punch roundings, lubrication conditions and blank holder forces have been considered.

Different examples of application to 2D and 3D sheet stamping problems are presented and compared with available experimental results.

1. INTRODUCTION

The flow approach is capable of predicting accurately, in a simple manner, changes in bulk and sheet geometry during the stamping processes, the load-displacement history and the distribution of strains and thicknesses at each deformation stage. Strain hardening, friction phenomena and localization effects due to microscopic void growth are also taken into account in this model.

Considerable attention is also given to the appropriate form of the material constitutive laws with the flow properties dependent on strain rate and temperature distributions. Elastic spring-back effects and residual stresses are predicted by means of a large-strain elasto-viscoplastic finite element model recently proposed for this class of problem involving large deformations and changes in geometry.

Many different finite element based codes for sheet forming analysis have been developed world-wide. There is a great dispersion of the basic approaches, constitutive equations, finite element models, solution strategies, etc. chosen for each of these codes. The need for code benchmarking is obvious and here the successes of different initiatives of this kind [5, 6, 7] point out a direction to be followed in the near future.

The paper consists of seven sections. After the Introduction, a number of basic equations of the flow approach and comments on solution algorithms are provided in Section 2.

Section 3 presents briefly the author's contribution to the numerical implementation of the very well known Coulomb model of friction in the specific case of the double side contact problem in the blank holder zone.

In Section 4, the possibility of predicting spring-back effects is investigated.

Information about a wide experimental program carried out by the author in a sheet stamping factory is provided in Section 5.

Section 6 contains a comparative study on sheet metal forming by numerical modelling and experiment.

In Section 7 conclusions are presented.

2. BASIC EQUATIONS

This approach is typical of fluid mechanics where a fixed Eulerian frame defining a control volume through which the material flows is used. This method appears to be more natural for bulk forming problems like mould filling, rolling, extrusion, etc. [25]. However, it can also be applied to stamping problems in a straightforward manner simply by identifying the control volume with the sheet geometry at each deforming step [9, 10, 11, 13].

The main variables of the flow approach are the *velocities* $\dot{\mathbf{u}}$ of the points of the deformed sheet and these are linearly related to the rates of deformation $\dot{\boldsymbol{\epsilon}}$ by

$$\dot{\boldsymbol{\epsilon}} = \mathbf{L}\dot{\mathbf{u}} \tag{1}$$

where $\mathbf{L}$ is the standard strain rate operator, i.e. for 2D problems

$$\mathbf{L} = \begin{bmatrix} \frac{\partial}{\partial x} & 0 \\ 0 & \frac{\partial}{\partial y} \\ \frac{1}{2}\frac{\partial}{\partial y} & \frac{1}{2}\frac{\partial}{\partial x} \end{bmatrix}. \tag{2}$$

The constitutive equation for the flow approach is usually written in the form

$$\mathbf{s} = \mathbf{D}\dot{\boldsymbol{\epsilon}}. \tag{3}$$

Equation (3) is typical of fluid mechanics where $\mathbf{s}$ is the stress deviator and $\mathbf{D}$ is the constitutive matrix dependent on flow viscosity only.

It can be shown that Eq. (1) is readily obtained for rigid plastic-viscoplastic materials. In the isotropic case, matrix $\mathbf{D}$ is a function of a single nonlinear flow viscosity parameter μ given for a rigid-plastic Huber-Mises material [25]

$$\mu = \frac{\sigma_y}{3\dot{\bar{\varepsilon}}} \tag{4}$$

where σ_y is the Huber-Mises yield stress and $\dot{\bar{\varepsilon}} = (\frac{2}{3}\dot{\varepsilon}_{ij}\dot{\varepsilon}_{ij})^{\frac{1}{2}}$. The expression of μ for viscoplastic materials including the effect of microscopic voids can be found in [1, 3]. It should also be noted that a cut-off value of μ must be used in quasi-rigid zones where $\dot{\bar{\varepsilon}} \simeq 0$ in order to prevent singularity.

The set of equations for the flow approach is completed with the equation for virtual work rate written as

$$\int_V \delta\dot{\boldsymbol{\epsilon}}^T \boldsymbol{\sigma}\, \mathrm{d}V = \int_V \delta\dot{\mathbf{u}}^T \mathbf{b}\, \mathrm{d}V + \int_\Gamma \delta\dot{\mathbf{u}}^T \mathbf{t}\, \mathrm{d}\Gamma \tag{5}$$

where $\boldsymbol{\sigma}$ is the Cauchy stress vector, $\mathbf{b}$ and $\mathbf{t}$ are body forces and surface tractions acting on the sheet volume V and surface Γ, respectively.

The form of the Huber-Mises constitutive equation (4) defines an incompressible flow problem (i.e. $\dot{\varepsilon}_{ii} = 0$). This induces serious difficulties if the finite element solution is based on "continuum" elements. However, the incompressibility condition can easily be imposed on "shell type" elements by setting the Poisson ratio at 0.5 and then updating the element thickness making use of the plane stress condition.

It is interesting to note that the general equations of the flow approach as written in (1)–(5) are analogous to those of standard infinitesimal (incompressible) elasticity. This analogy can be exploited to simplify further the computational procedure by using directly standard finite element codes written for the elasticity case in which displacements and strains are simply replaced by velocities and strain rates, respectively, and the shear modulus by the (nonlinear) flow viscosity [9, 10, 11, 13, 25].

The velocity field is discretized in the standard form

$$\dot{\mathbf{u}} = \mathbf{N}\dot{\mathbf{a}} \tag{6}$$

where $\mathbf{N}$ and $\dot{\mathbf{a}}$ are the shape function matrix and the nodal velocity vector, respectively [26].

Some of the elements currently used in the context of the flow approach include:

Plane strain bending element: Two-node linear elements based on the Timoshenko beam theory have been chosen. Such an element can easily be simplified to a two-node membrane element.

Axisymmetric shell element: Two-node linear axisymmetric shell element based on the Reissner-Mindlin axisymmetric shell theory has been selected [9, 10, 11, 13, 26]. Again this element can easily be simplified to the standard two-node axisymmetric membrane element.

3D shell elements: Different thin shell elements based on the facet shell theory are used [26]. These include the simple DKT and Morley triangles [26] as well as a new three node bending element with only translational degrees of freedom recently developed by Oñate et al. [9]. Both full bending and membrane cases are considered.

After discretization, the resulting nonlinear equilibrium equation can be written in the form [26]

$$\mathbf{r}(\dot{\mathbf{a}}, \mathbf{x}, t) = \mathbf{p}(\dot{\mathbf{a}}, t) - \mathbf{f}(t, \mathbf{x}) = \mathbf{0} \tag{7}$$

where $\mathbf{r}$, $\mathbf{p}$ and $\mathbf{f}$ stand for the vectors of residual forces, internal forces and external forces, respectively, $\mathbf{x}$ is the cartesian coordinate vector and t is the time. The vector $\mathbf{p}$ can be written in the flow approach as

$$\mathbf{p} = \mathbf{K}\dot{\mathbf{a}} \quad \text{with} \quad \mathbf{K} = \int_V \mathbf{B}^T \mathbf{D} \mathbf{B} \, \mathrm{d}V \,. \tag{8}$$

In (8), $\mathbf{K}$ is the stiffness matrix obtained from the constitutive matrix of Eq. (3) and the strain rate matrix $\mathbf{B}$ [9, 10, 11, 13].

Equation (7) can be solved iteratively for the values of $\dot{\mathbf{a}}$. For the k-th iteration we have

$$\Delta\dot{\mathbf{a}}^k = -\left[{}^{t+\Delta t}\mathbf{H}^k\right]^{-1} {}^{t+\Delta t}\mathbf{r}^k \tag{9}$$

where $\mathbf{H}$ is an adequate iteration matrix. The vector $\dot{\mathbf{a}}$ is subsequently updated as

$${}^{t+\Delta t}\dot{\mathbf{a}}^{k+1} = {}^{t+\Delta t}\dot{\mathbf{a}}^k + \Delta\dot{\mathbf{a}}^k .$$

The next step is to compute the new stress field with Eq. (3). Then the sheet geometry and mechanical properties are updated and the sheet-tool contact and friction condition is checked. The process is restarted and it continues until convergence is achieved. It has been established that a convergence norm based on velocities is more appropriate than one based on residual forces. Details of this fact are given in [20]. This is due to the cut-off value for viscosity in quasi-rigid body zones which can lead to inaccurate stress values in these regions.

Details on the choice of the iteration matrix $\mathbf{H}$ and on different geometry updating procedures available can be found in [10].

3. FRICTIONAL CONTACT

Contact and friction appear as a consequence of the interaction between the sheet and the tools. The numerical treatment of frictional contact involves two main steps. First, a *contact search* must be performed in order to detect the penetration between the sheet and the tools. Using the slave-master methodology it is imposed that the slave nodes do not penetrate the master surface. This involves a search procedure to detect if penetration has taken place. Special care must be taken if the search is done using the element normal vectors in order to treat different situations arising from the normal vector field in facet type elements [12].

The contact problem is dealt with in this paper by means of the penalty method [14, 24] due to its simplicity. Alternative approaches can be found in other works [14, 16]. Frictional effects have been described by means of the Coulomb model with some numerical modifications described in [17, 18, 20, 21]. A plasticity theory framework is found very adequate for the derivation of consistent tangent operators [2, 14].

4. SPRING-BACK EFFECTS

The computation of spring-back effects is important in sheet stamping operations. In principle, only finite element computations incorporating elastic effects in the constitutive equations (i.e. elastoplastic or elasto-viscoplastic models) can deal with elastic recovery effects in a straightforward manner.

The author has investigated the possibility of predicting spring-back effects by means of a rigid-plastic-viscoplastic flow formulation with the following procedure:

a) During the loading process the effects of elasticity are neglected in all elements and the flow formulation is used as previously described.

b) Once the tools are removed the sheet is assumed to behave elastically. This simply implies replacing the original constitutive matrix $\mathbf{D}(\mu)$ by that of standard elasticity $\mathbf{D}(E,\nu)$ where E is the Young modulus and ν the Poisson ratio, and interpreting the velocity vector $\dot{\mathbf{a}}$ as the displacement vector $\mathbf{a}$. Basic equations of the problem remain unchanged according to the famous flow approach–solid approach analogy [25].

c) Equilibrium under the initial stress field is obtained by means of the updated Lagrangian iterative approach accounting for geometrically nonlinear effects. The simplest iterative process can be written in the form

$$\boldsymbol{\sigma}^k = \boldsymbol{\sigma}^\circ \quad \text{for} \quad k = 1\,, \tag{10}$$

$$\Delta\mathbf{a}^k = -\mathbf{K}^{-1}\int_V [\mathbf{B}^k]^T\boldsymbol{\sigma}^k\,\mathrm{d}V\,, \tag{11}$$

$$\mathbf{a}^{k+1} = \mathbf{a}^k + \Delta\mathbf{a}^k, \tag{12}$$

$$\boldsymbol{\sigma}^{k+1} = \boldsymbol{\sigma}^k + \mathbf{D}\mathbf{B}^k\Delta\mathbf{a}^k, \tag{13}$$

where $\boldsymbol{\sigma}^\circ$ is the initial stress obtained in the last increment during the stamping process by means of the flow approach, $\mathbf{K}$ is the elastic stiffness matrix, kept constant during the iterations and $\mathbf{B}^k$ is the standard strain matrix based on the small displacement theory and updated for each iteration. The iterative process stops when the residual forces equal to $-\int \mathbf{B}^T\boldsymbol{\sigma}\,\mathrm{d}V$ satisfy a prescribed norm. This process can be enhanced by scaling the initial stresses which are then applied in an incremental manner.

5. DESCRIPTION OF BRITE EXPERIMENT

5.1. Experiment design and methodology

The objective of this section is to present some of the results of experimental tests which have been performed in Spain, in a stamping factory, Estampaciones Sabadell S.A., with cylindrical and prismatic dies designed and manufactured at Candemat S.A.

The tests included the deep drawing of circular and rectangular blanks with cylindrical and prismatic dies, respectively.

A total of 29 successful tests have been performed. Unsuccessful tests included those with drawing depth much smaller than the value corresponding to the ultimate strength or maximum displacement possible, or those in which total collapse of the blank has been reached. Only two test results are presented in this paper. The full report [21] has already been published.

Different die and punch edge radii (i.e. roundings), the use of different lubrication conditions in the whole contact area and of different blank holding forces have been included in the experimental study.

The blank geometry data, i.e. draw-in values on boundaries, drawing depth and thickness distribution, have been measured after each test.

As it was observed in the stamping factory, the maximum drawing depth possible before the blank collapse depended on deep drawing parameters such as blank holder pressure, friction coefficient (with or without oil on tool surfaces), punch speed, geometry of tools and the quality of the blank material.

In [21] a small Fortran program calculating the distance between measuring points and the deformed blank symmetry centre as a function of tool roundings, drawing depth and final dimensions for each symmetry line is given.

5.2. Data and results

Three types of material have been used: AP04XR, series of 17.06.1991 (material 1), of 31.01.1992 (material 3) for circular blanks and series of 13.09.1991 (material 2) for rectangular blanks.

Standard tension tests were applied with the use of the testing machine HOYTOM DI-10-CP/SV in order to establish tension characteristics for each material. In the case of circular blanks, eight test pieces presented in Fig. 1 were cut off from the panel in different directions. In the case of rectangular blanks, similar eight test pieces were cut off in two directions parallel to panel sides and in two diagonal directions. The results of one of the tension tests carried on up to collapse for each test piece are presented for material 2 for rectangular blank in Fig. 2.

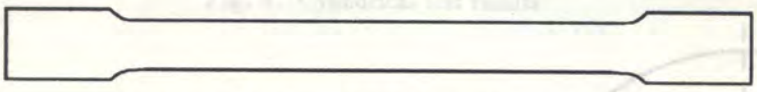

Fig. 1. Specimen for material tension test

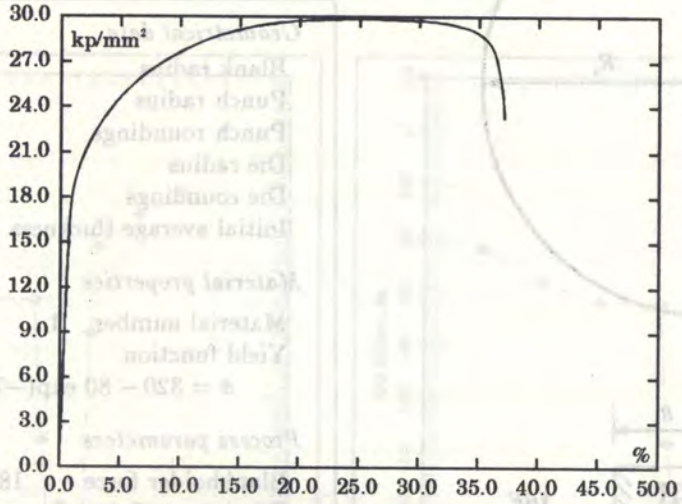

Fig. 2. Results of one typical material tension test

It was observed that the dispersion of different curves characterizing material behaviour for the circular blank is greater than in the case of the rectangular blank. Thus, the quality of material for rectangular tests was higher.

It must be admitted here that the initial thickness distribution measured before experiments for some blanks shows relatively big dispersion. The differences between maximum and minimum values of initial thickness in some cases are greater than the differences between values in post-experimental thickness distribution, especially when the maximum drawing depth reached before collapse was relatively small (in the range of 10–20 mm in experiments without oil).

A constant blank holder force (BH) corresponding to the initial contact area between the blank holder and the blank was applied:

A. for the cylindrical test:

blank holder pressure 60 kp/cm^2,

area of initial contact between BH and sheet: 317.6 cm^2,

BH Force = 19 061.64 kp = 186 995 N.

B. for the prismatical test:

blank holder pressure 75 kp/cm^2,

area of initial contact between BH and sheet: 326.74 cm^2,

BH Force = 24 505.5 kp = 240 402 N.

Two different lubrication conditions on tool and blank surfaces, with oil and without oil, have been considered in the experiments. However, the exact value of friction coefficients is unknown.

Let us call x and y the friction coefficients corresponding to oil lubrication and dry friction conditions, respectively. This notation has been used in the description of process parameters in data given for each test in Figs. 3 and 6.

Data summary and all the results obtained are collected for two tests in Figs. 3–5 (for the cylindrical test) and in Figs. 6–9 (for the prismatic test).

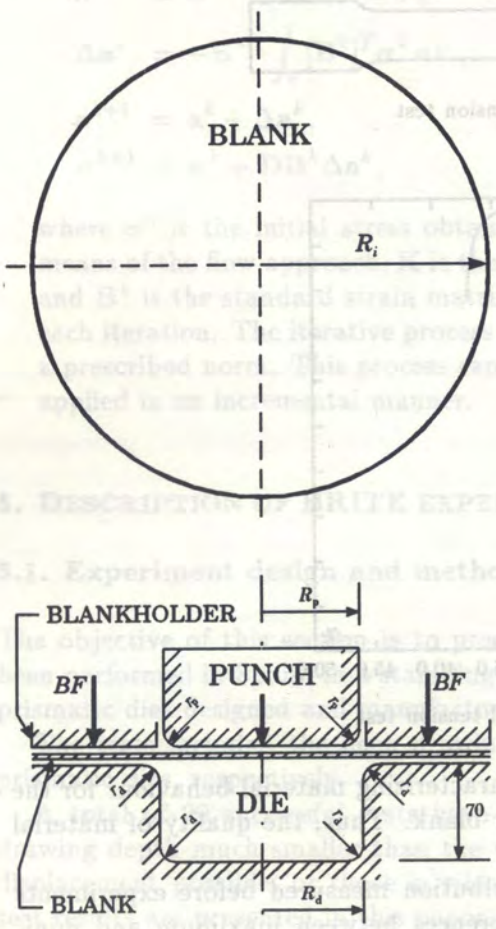

Geometrical data

Blank radius	250.0 mm
Punch radius	149.9 mm
Punch roundings	9.0 mm
Die radius	150.7 mm
Die roundings	9.0 mm
Initial average thickness	0.687 mm

Material properties

Material number 1

Yield function

$$\bar{\sigma} = 320 - 80 \exp(-7.5\varepsilon^{0.97})$$

Process parameters

Blankholder force	186 995 N/quarter
Friction coefficient	x
Punch displacement	32.0 mm

Fig. 3. Cylindrical test data

Meas. point	Thickness, mm	
	Edge $Y = 0$	Edge $X = 0$
1	.690	.690
2	.689	.689
2	.686	.686
4	.684	.684
5	.684	.684
6	.671	.671
7	.661	.661
8	.665	.665
9	.661	.661
10	.660	.660
11	.681	.681
12	.689	.689
13	.692	.692
14	.694	.694
15	.700	.700

Other measured results

Specimen	L
Final diameter, edge $Y = 0$	467.3 mm
Final diameter, edge $X = 0$	468.5 mm

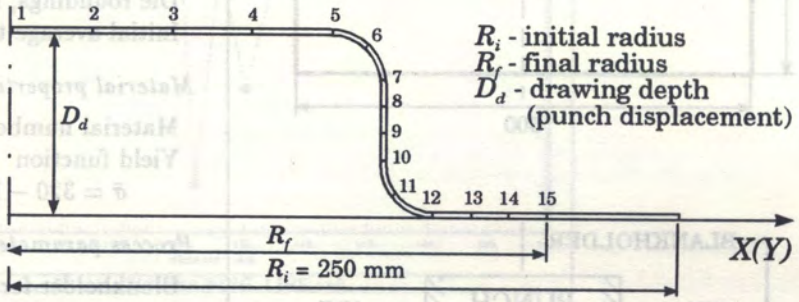

Fig. 4. Cylindrical test results

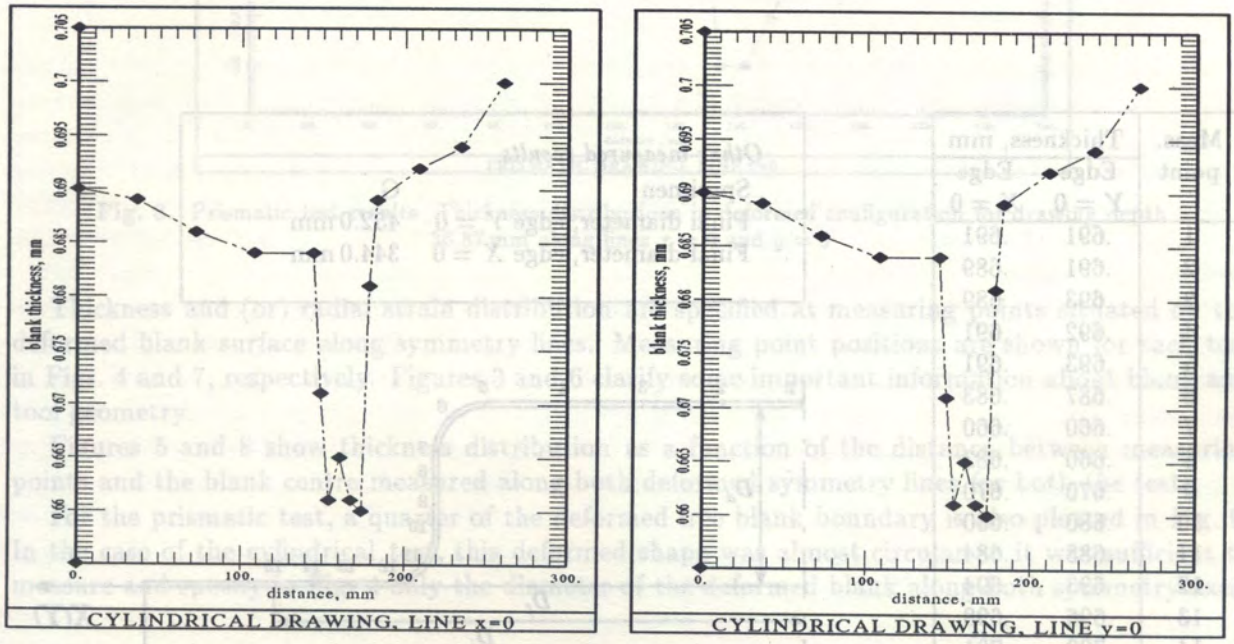

Fig. 5. Cylindrical test results. Thickness distributions in deformed configuration for drawing depth 32.0 mm along lines $x = 0$ and $y = 0$

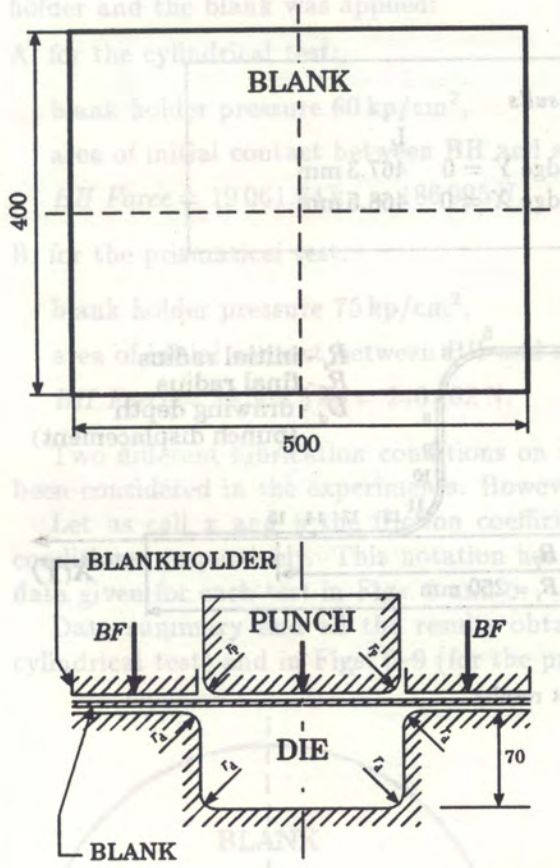

Geometrical data

Initial blank dimensions	400.0 × 500.0 mm
Punch dimensions	100.0 × 150.0 mm
Punch roundings, r_p	6.0 mm
Die dimensions	100.7 × 150.7 mm
Die roundings, r_d	6.0 mm
Initial average thickness	0.70 mm

Material properties

Material number 2

Yield function

$$\bar{\sigma} = 320 - 195 \exp(-7.5\varepsilon^{0.97})$$

Process parameters

Blankholder force, BF	240 402 N/quarter
Friction coefficient	x
Drawing depth, D_d (Punch displacement)	36.87 mm

Fig. 6. Prismatic test data

Meas. point	Thickness, mm	
	Edge $Y = 0$	Edge $X = 0$
1	.691	.691
2	.691	.689
2	.693	.689
4	.692	.691
5	.693	.691
6	.687	.683
7	.660	.660
8	.660	.683
9	.670	.670
10	.680	.680
11	.688	.684
12	.693	.694
13	.696	.698
14	.709	.701
15	.722	.708

Other measured results

Specimen	G
Final diameter, edge $Y = 0$	452.0 mm
Final diameter, edge $X = 0$	344.0 mm

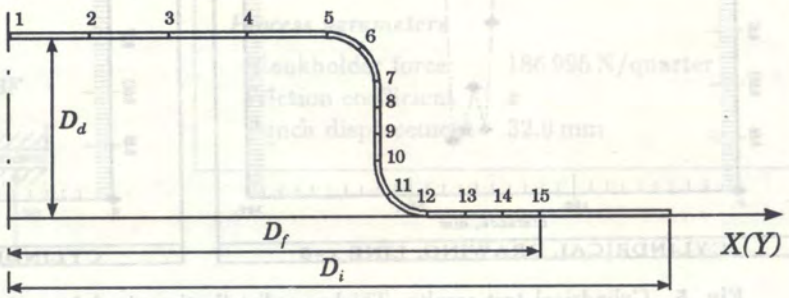

Fig. 7. Prismatic test results

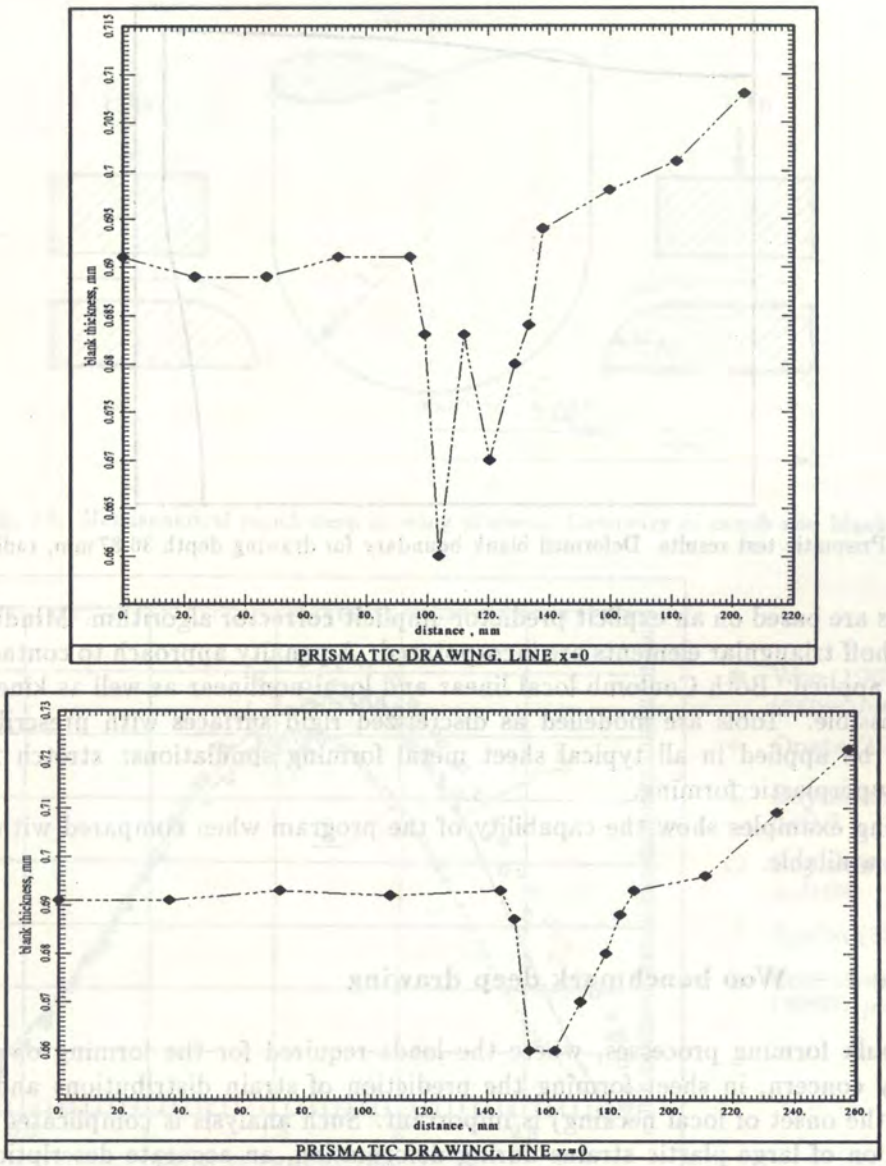

Fig. 8. Prismatic test results. Thickness distributions in deformed configuration for drawing depth 36.87 mm along lines $x = 0$ and $y = 0$

Thickness and (or) radial strain distribution are specified at measuring points situated on the deformed blank surface along symmetry lines. Measuring point positions are shown for each test in Figs. 4 and 7, respectively. Figures 3 and 6 clarify some important information about blank and tool geometry.

Figures 5 and 8 show thickness distribution as a function of the distance between measuring points and the blank centre measured along both deformed symmetry lines for both the tests.

For the prismatic test, a quarter of the deformed free blank boundary is also plotted in Fig. 9. In the case of the cylindrical test, this deformed shape was almost circular so it was sufficient to measure and specify in Fig. 4 only the diameter of the deformed blank along both symmetry axes.

6. Numerical modelling versus experiment — examples

Starting from the approach described in [8] and in the previous sections, numerical codes MFP2D and MFP3D were developed and extended [4, 17, 18, 19, 20, 21, 22].

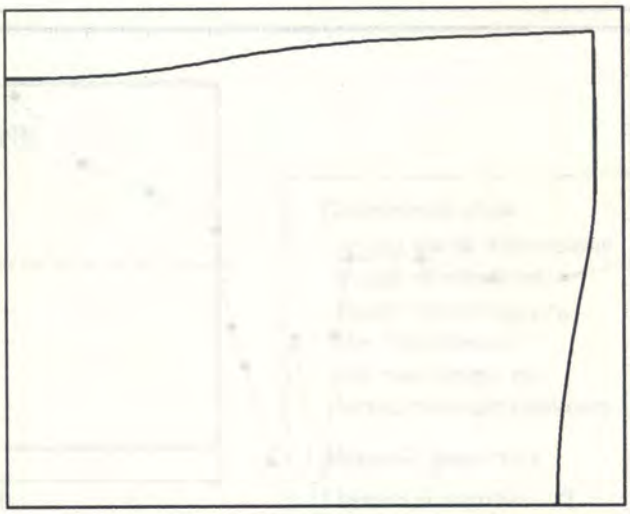

Fig. 9. Prismatic test results. Deformed blank boundary for drawing depth 36.87 mm, radius 6 mm

These codes are based on an explicit predictor–implicit corrector algorithm. Mindlin 2-node and discrete Kirchhoff triangular elements are incorporated. A penalty approach to contact and friction phenomena is applied. Both Coulomb local linear and local nonlinear as well as kinematic friction models are possible. Tools are modelled as discretized rigid surfaces with prescribed velocities. Programs can be applied in all typical sheet metal forming simulations: stretch forming, deep drawing and superplastic forming.

The following examples show the capability of the program when compared with some experimental results available.

6.1. Example 1 — Woo benchmark deep drawing

Unlike most bulk forming processes, where the loads required for the forming operation are often of primary concern, in sheet forming the prediction of strain distributions and limit strains (which define the onset of local necking) is important. Such analysis is complicated as it requires the consideration of large plastic strains during deformation, an accurate description of material response including strain hardening, the treatment of a moving boundary that separates the region in contact with the punch from the unsupported one, and the inclusion of friction between the sheet and the punch.

The deep drawing of a thin circular isotropic sheet with a hemispherical punch is considered in the first example in order to demonstrate the large strain capabilities of the axisymmetric and membrane 2D elements. The experimental results are available for this very well known benchmark [23].

The geometrical configuration of the problem is shown in Fig. 10. The initial radius of the blank is 2.22 inches. In the experiment, graphite in tallow was used for lubrication. Woo assumed that the coefficient of friction was 0.04.

Fifty linear bending elements have been used for the analysis. The analysis was performed with the use of the 2D version of the program with axisymmetric algorithm option.

The uniaxial stress–effective strain curve of the matrix material is given by

$$\sigma = 5.4 + 27.8\varepsilon^{0.504} \frac{\text{ton}}{\text{in}^2}, \qquad \varepsilon < 0.36\,, \tag{14}$$

$$\sigma = 5.4 + 24.4\varepsilon^{0.504} \frac{\text{ton}}{\text{in}^2}, \qquad 0.36 < \varepsilon\,. \tag{15}$$

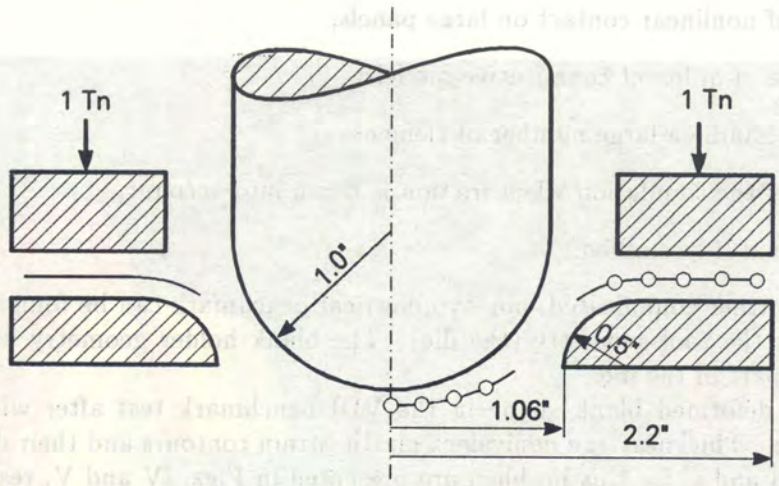

Fig. 10. Hemispherical punch deep drawing problem. Geometry of punch and blank

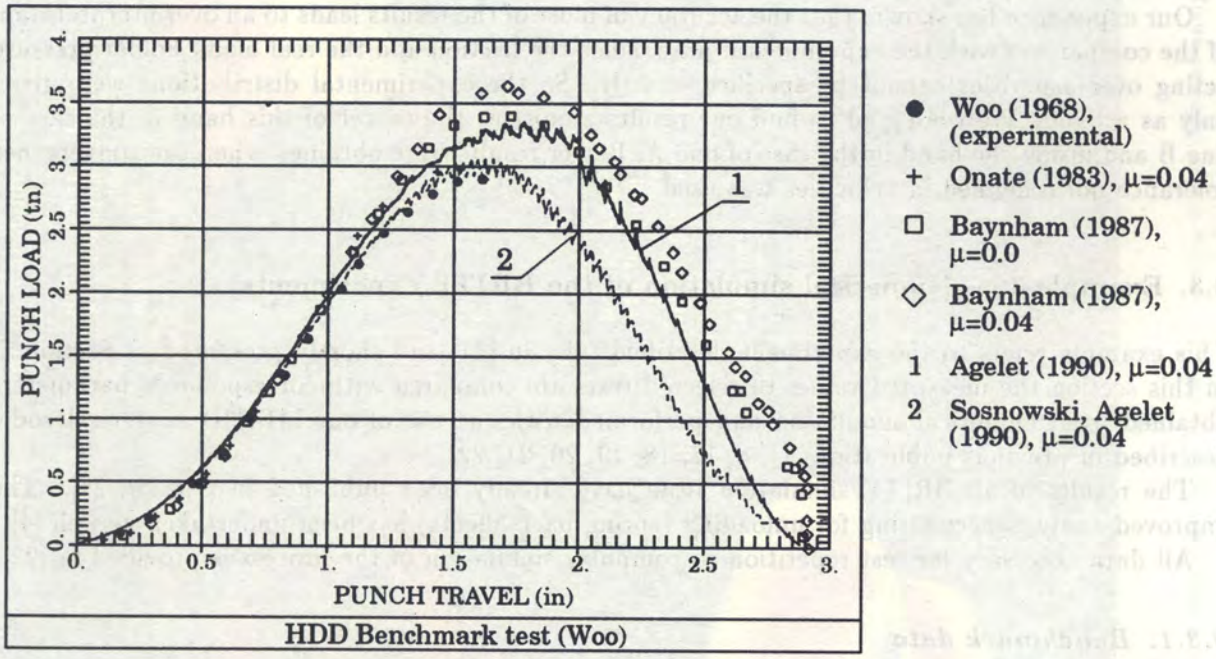

Fig. 11. Hemispherical punch deep drawing. Punch load-displacement curves obtained by different authors

Figure 11 shows the results for the punch load–displacement curves obtained for zero porosity and the friction coefficient of 0.04 by different authors and compared with experimental results. Both the old and the new improved version of our program were used in the analysis. The numerical results reported for this problem are much closer to experiment now.

The deformed shapes at two different analysis stages, thickness and equivalent plastic strain distribution are presented in Fig. I.

6.2. Example 2 — VDI (Zurich) benchmark

The goal of this benchmark was to prove the applicability of different codes to deliver accurate results for real industrial parts. In particular, the following objectives were pointed out:

a) the significant differences between explicit and implicit formulations,

b) the behaviour of nonlinear contact on large panels,

c) the formulations of different constitutive models,

d) the capacity to handle a large number of elements,

e) the behaviour of the simulation when friction is taken into account,

f) the computational time needed.

All details of this rather complicated, non-symmetrical benchmark can be found in [5].

Figure II shows the tool geometry (the die). The blank holder geometry was assumed to be similar to the flat part of the die.

In Fig. III the deformed blank shape in the VDI benchmark test after whole deep drawing process is presented. Thickness and equivalent plastic strain contours and their distributions along specified lines A, B and C for this problem are presented in Figs. IV and V, respectively. Figures 12 and 13 contain thickness distribution along lines A and B as reported in [17] by different authors and compared with our results.

Our experience has shown, that the accuracy of most of the results leads to an overinterpretation of the comparison with the experimental data, since the friction and the real blank holder pressure acting over asperities cannot be specified exactly. So the experimental distributions were given only as a band. We were glad to find our results almost at the center of this band in the case of line B and inside the band in the case of line A. Better results were obtained when the convergence tolerance norm defined in velocities was used.

6.3. Example 3 — Numerical simulation of the BRITE experiments

This example refers to the experiment described fully in [21] and shortly presented in Section 5. In this section the measured values of selected tests are compared with corresponding parameters obtained from numerical simulation and performed with the use of our MFP3D numerical code, described in previous publications [4, 8, 17, 18, 19, 20, 21, 22].

The results of all BRITE simulation tests have already been published in [19, 20, 21]. The improved analysis accounting for unloading (spring-back effects) has been undertaken as well [4].

All data necessary for test repetition or computer simulation of the process is provided in [22].

6.3.1. Benchmark data

Material properties

The material (steel) is assumed to satisfy the relation between true stress and strain as given in corresponding Figs. 3 and 6 for each test. For spring-back behaviour the Young modulus is 211 GPa and Poisson ratio is 0.3. With this data an initial yield stress of 81.3 MPa is obtained. The material in this process is fully isotropic.

Geometry

The initial average thickness assumed for numerical simulation data may be different from real average thickness with error up to 0.1 mm. Thickness measurements after experiment are given in Figs. 4 and 7. Figures 3 and 6 contain the average values taken for numerical simulation.

Tool geometry has been introduced into the MFP3D program as discretized rigid surfaces modelled with simple triangles. The coordinates of all points used in order to build images of tools for all five geometries consisting of die, punch and blank holder are given in [22].

The circular blank to be drawn has an initial radius of 250 mm and an initial thickness of 0.67 mm to 0.712 mm, depending on the test analyzed.

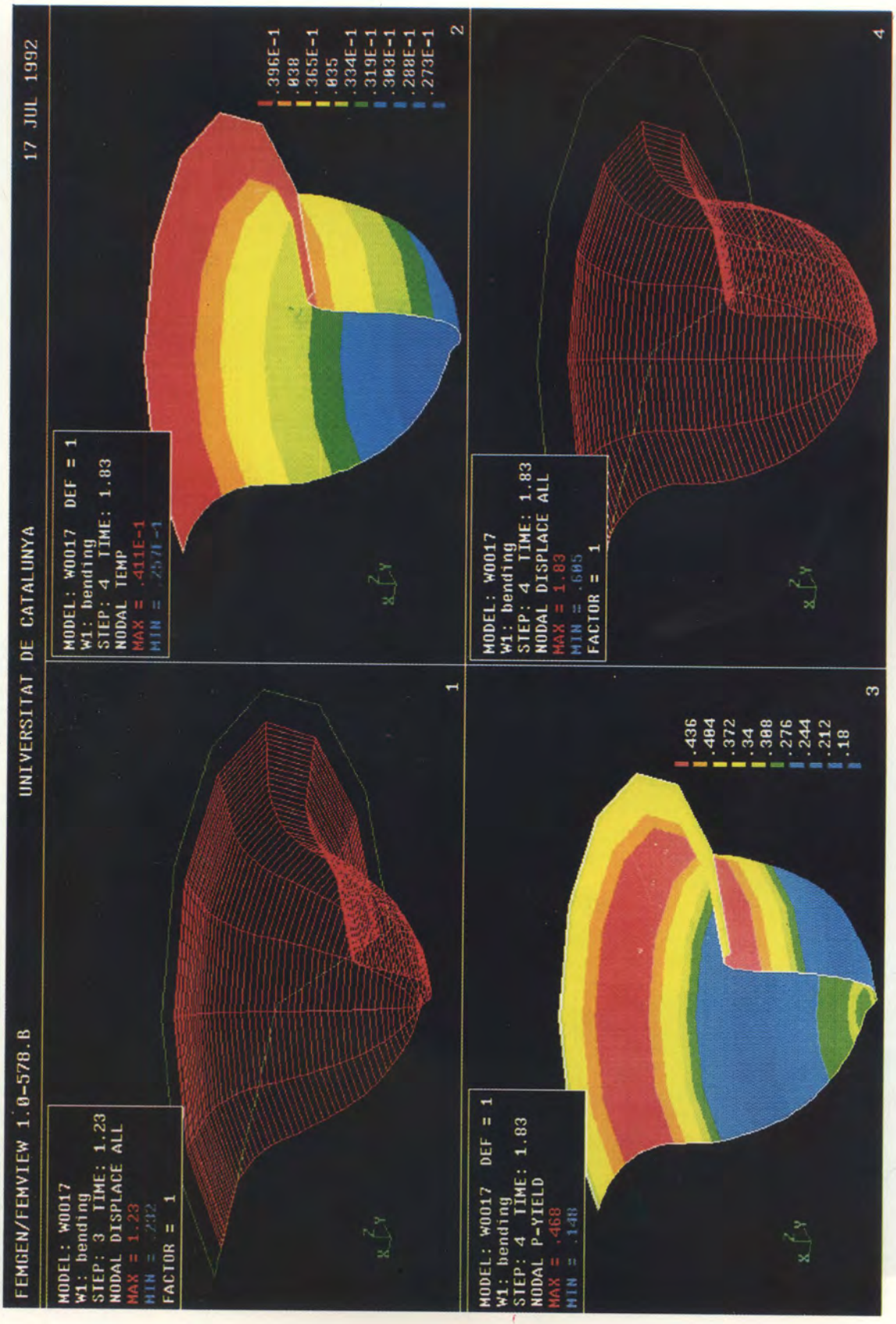

Fig. I. Hemispherical punch deep drawing. The deformed shapes at two different analysis stages, thickness and equivalent plastic strain distribution

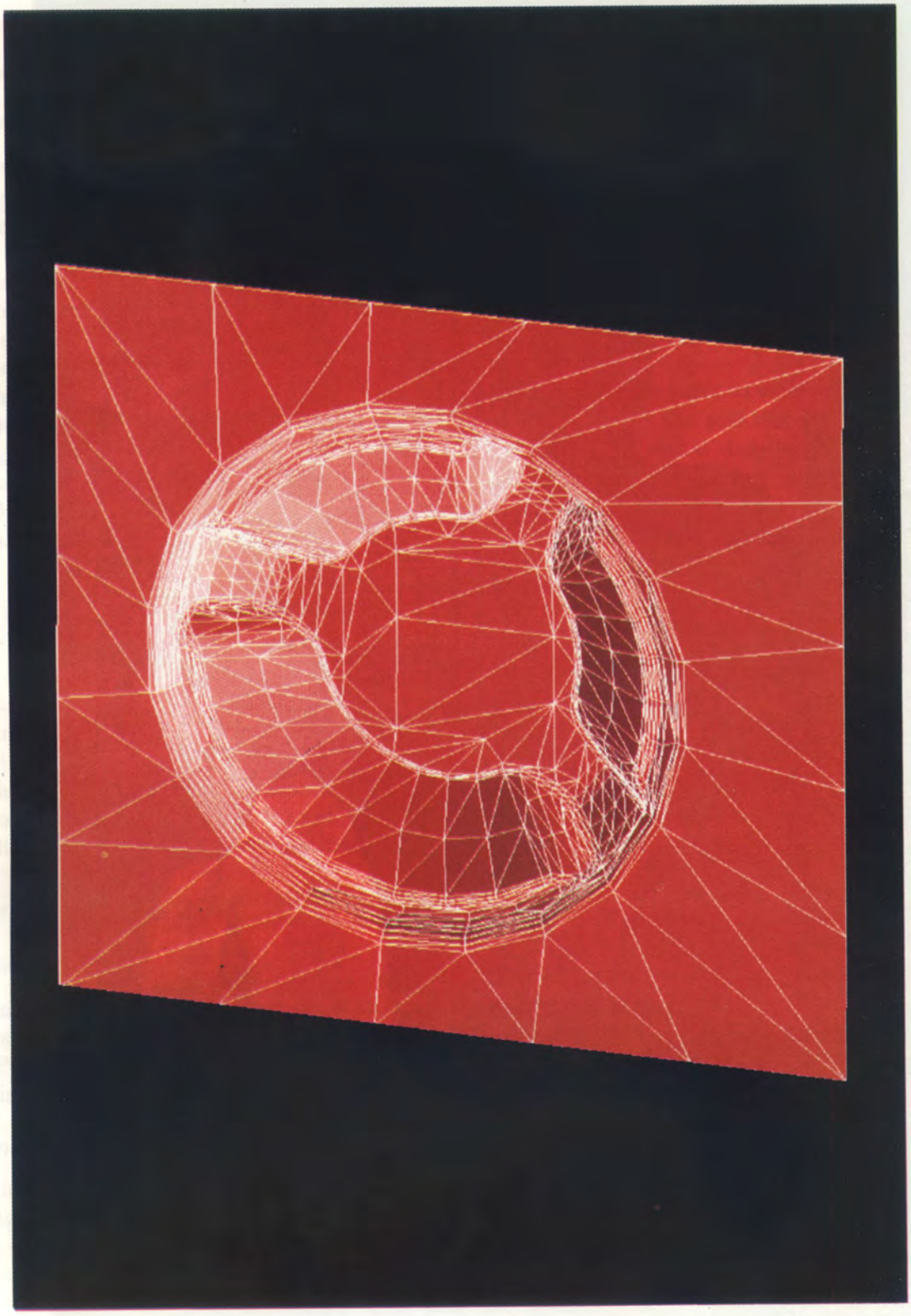

Fig. II. Tool (die) geometry for VDI benchmark test

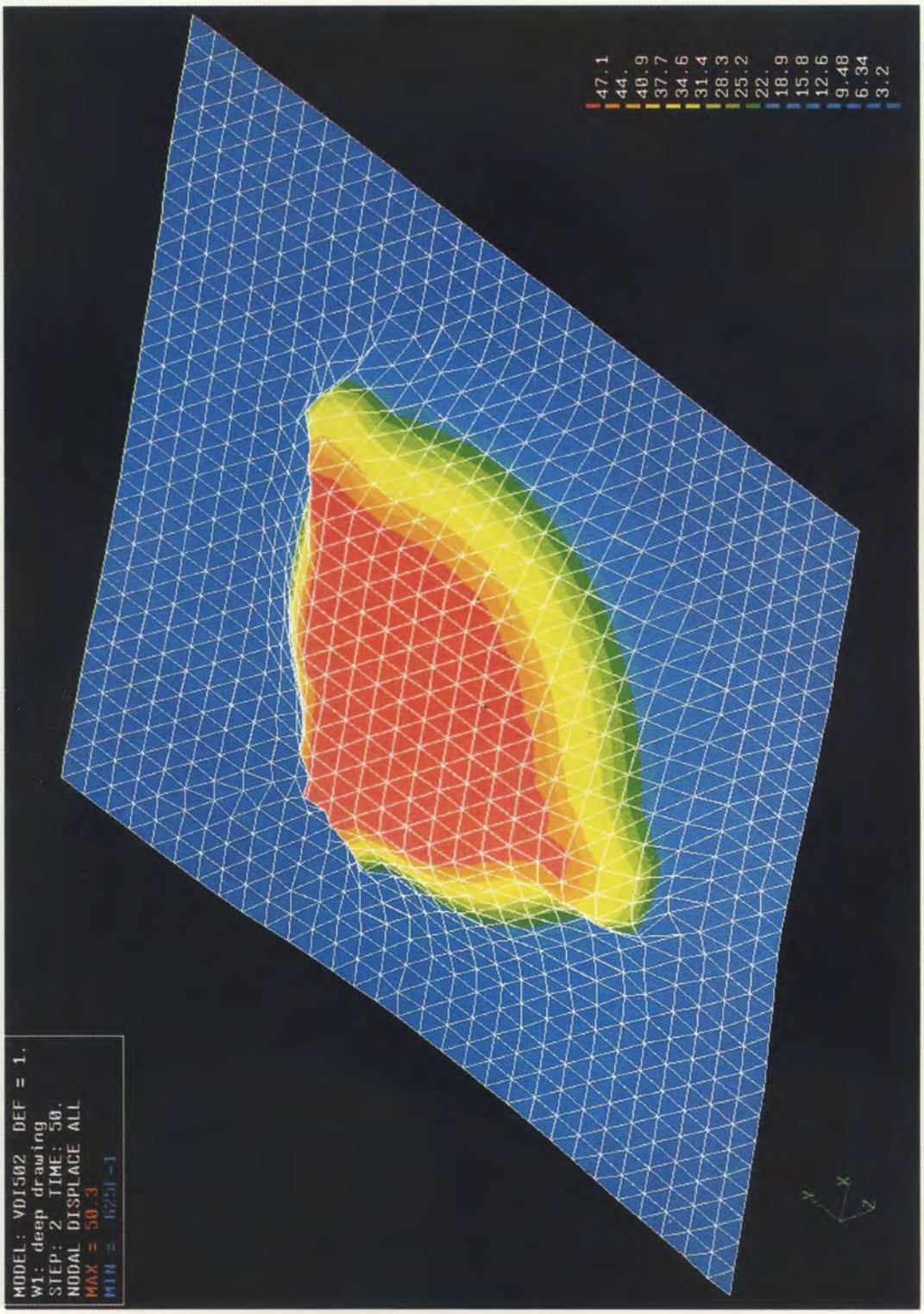

Fig. III. Deformed shape of the blank — displacement field

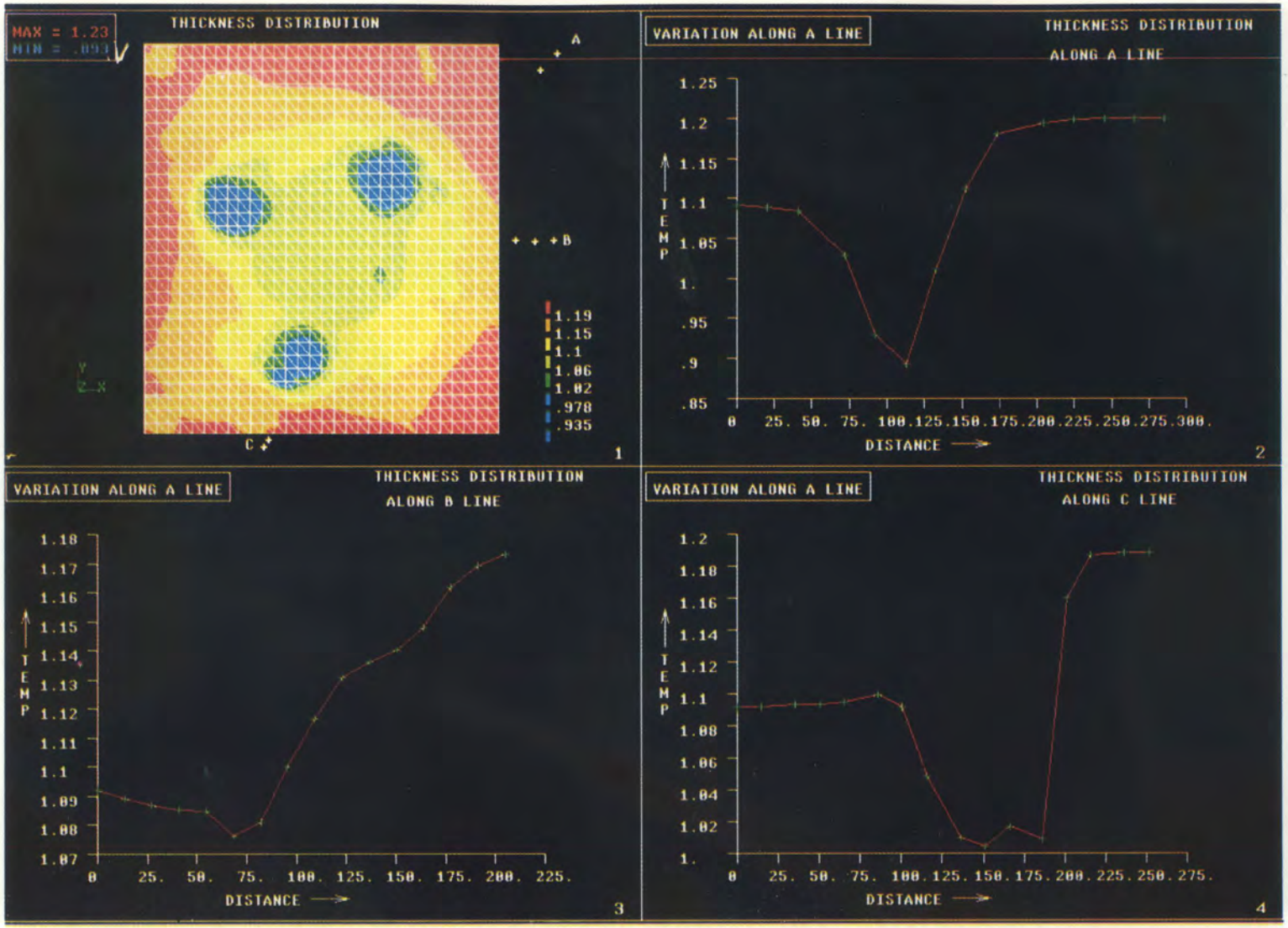

Fig. IV. VDI Benchmark — thickness along lines A, B and C

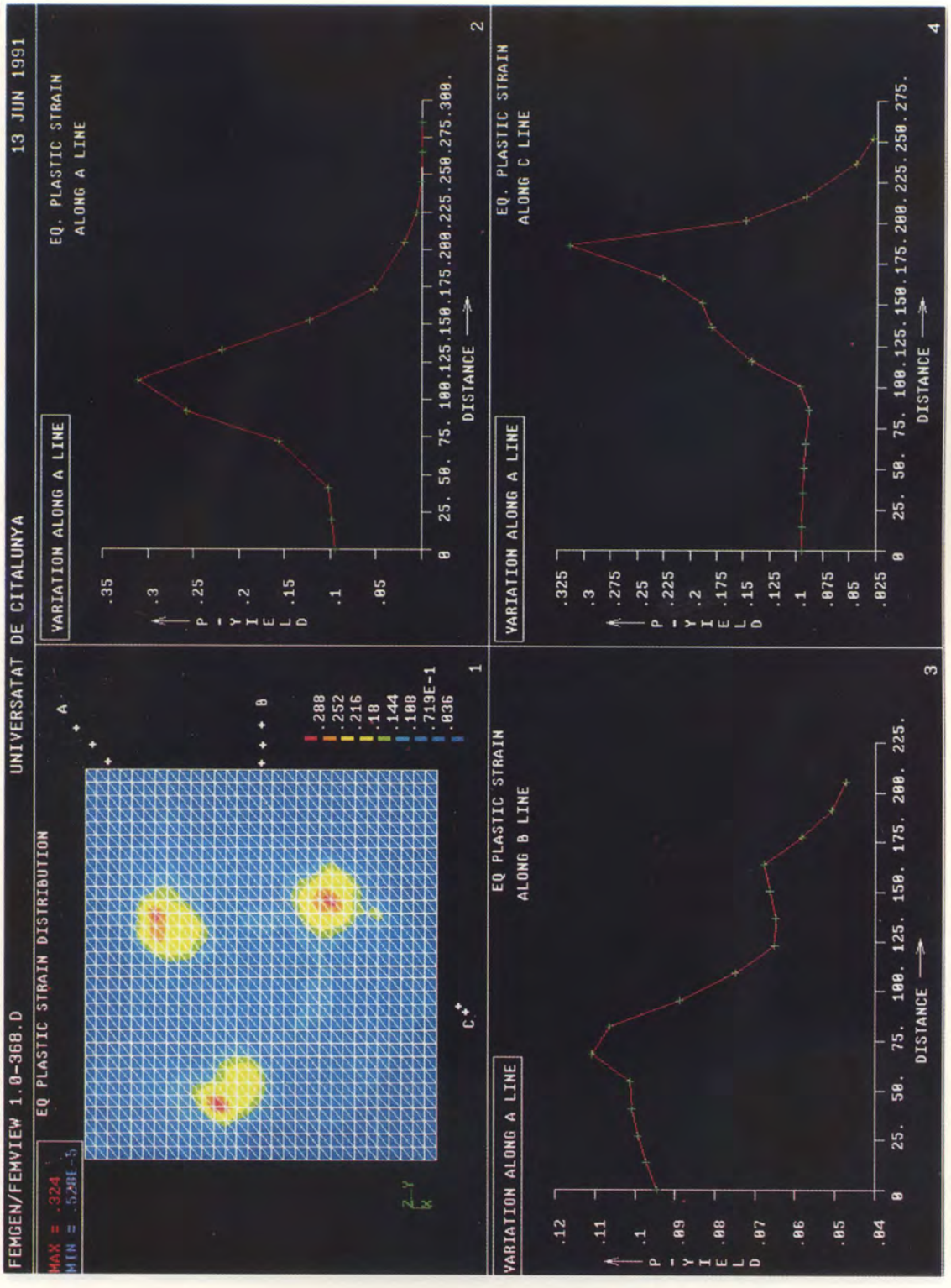

Fig. V. VDI benchmark — equivalent plastic strain

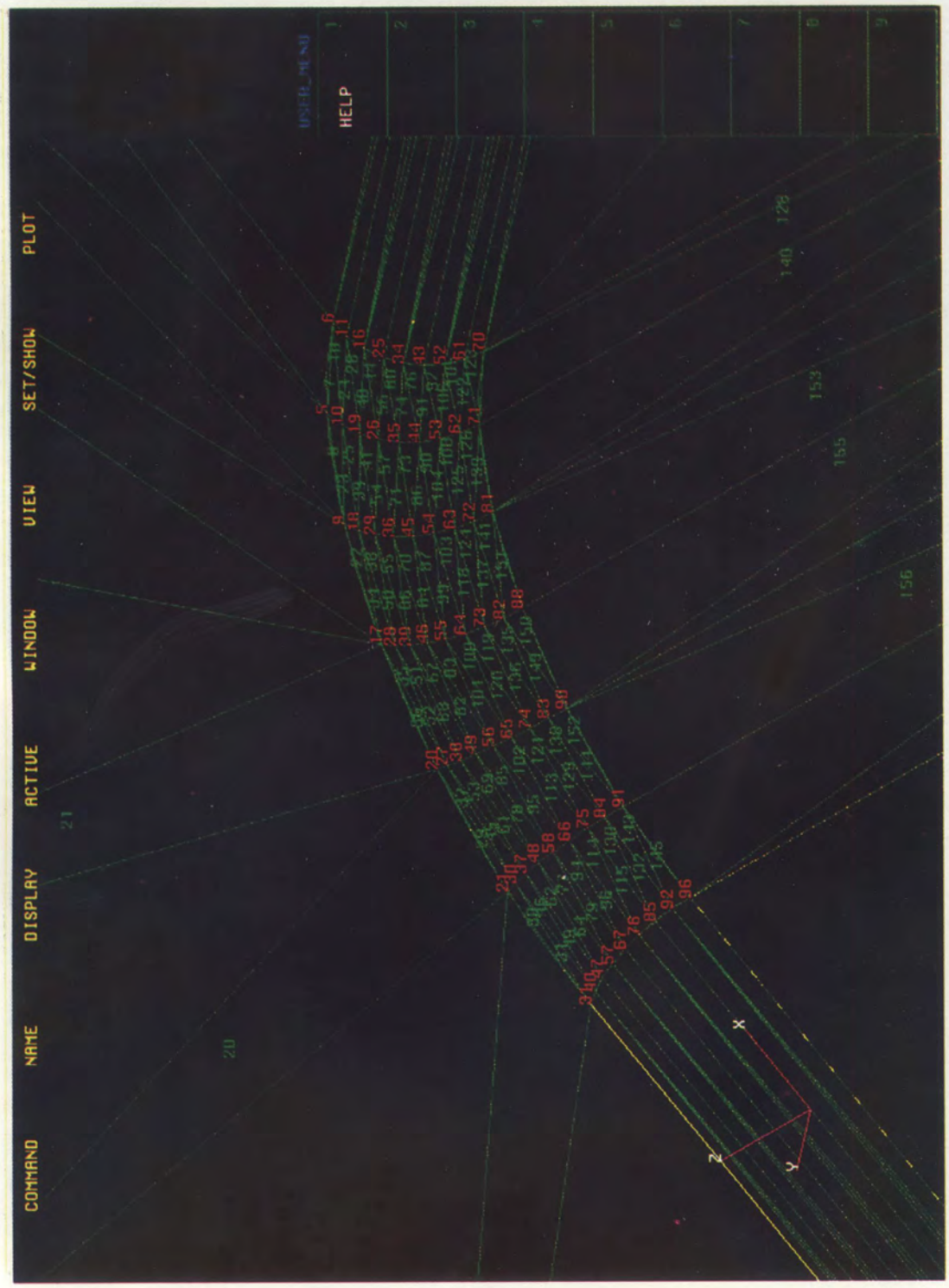

Fig. VI. BRITE tests. Discretization of a part of tool rounding

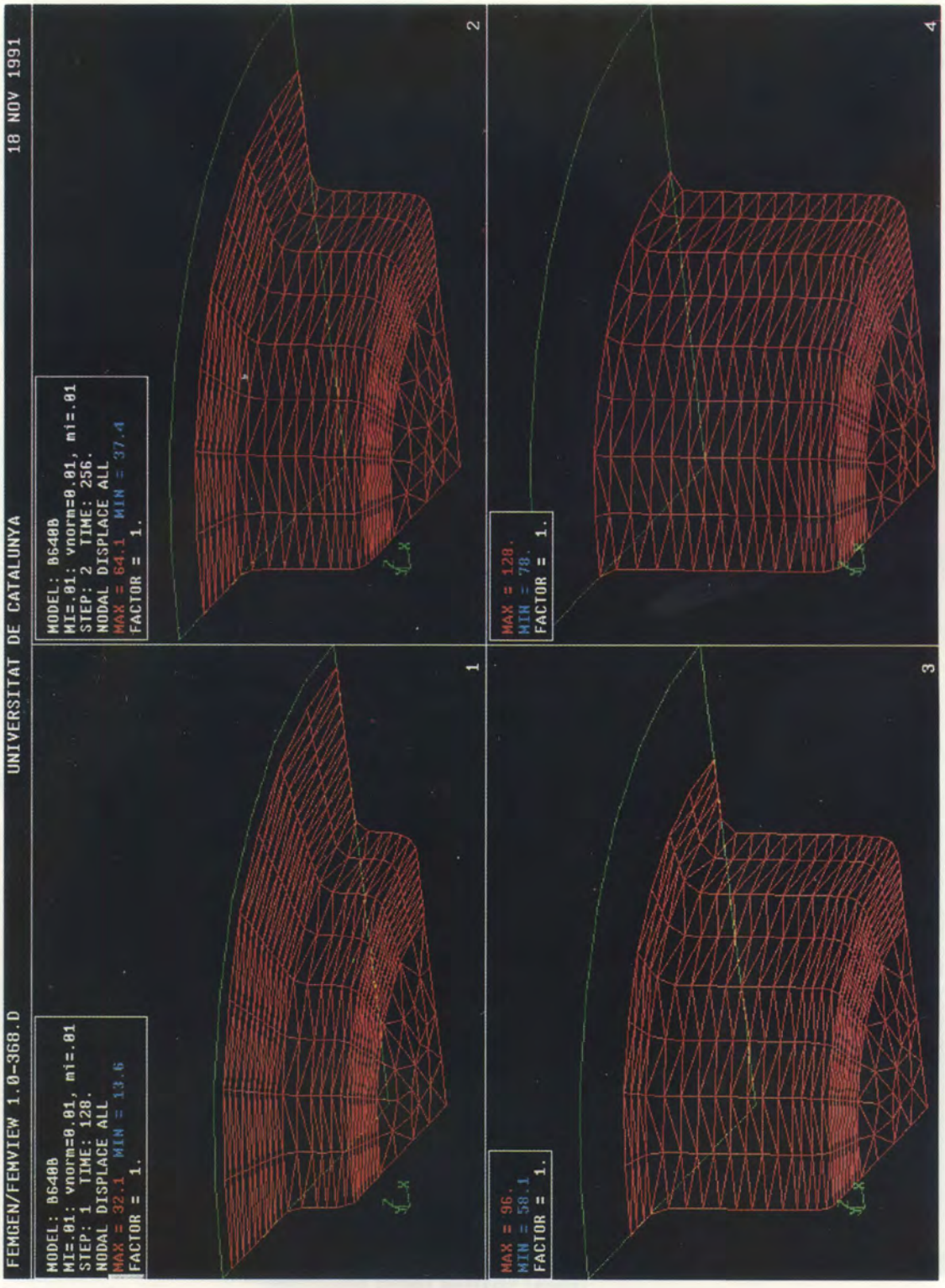

Fig. VII. BRITE tests. Calculated deformed shapes, configuration for time $t = 256$ sec. corresponding to test no. 10 [22]

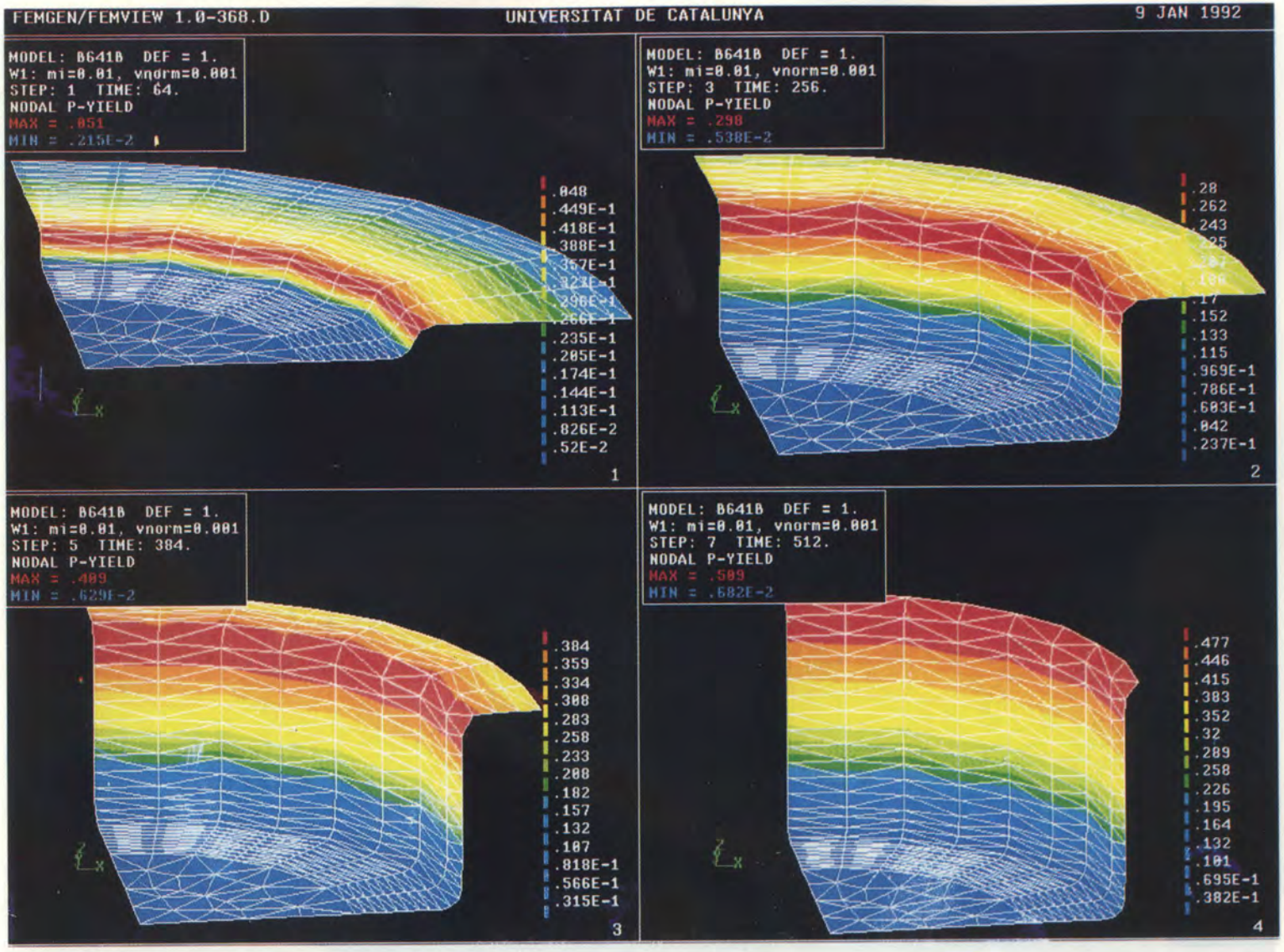

Fig. VIII. BRITE tests. Calculated thickness distribution, results for time $t = 256$ sec. corresponding to test no. 10 [22]

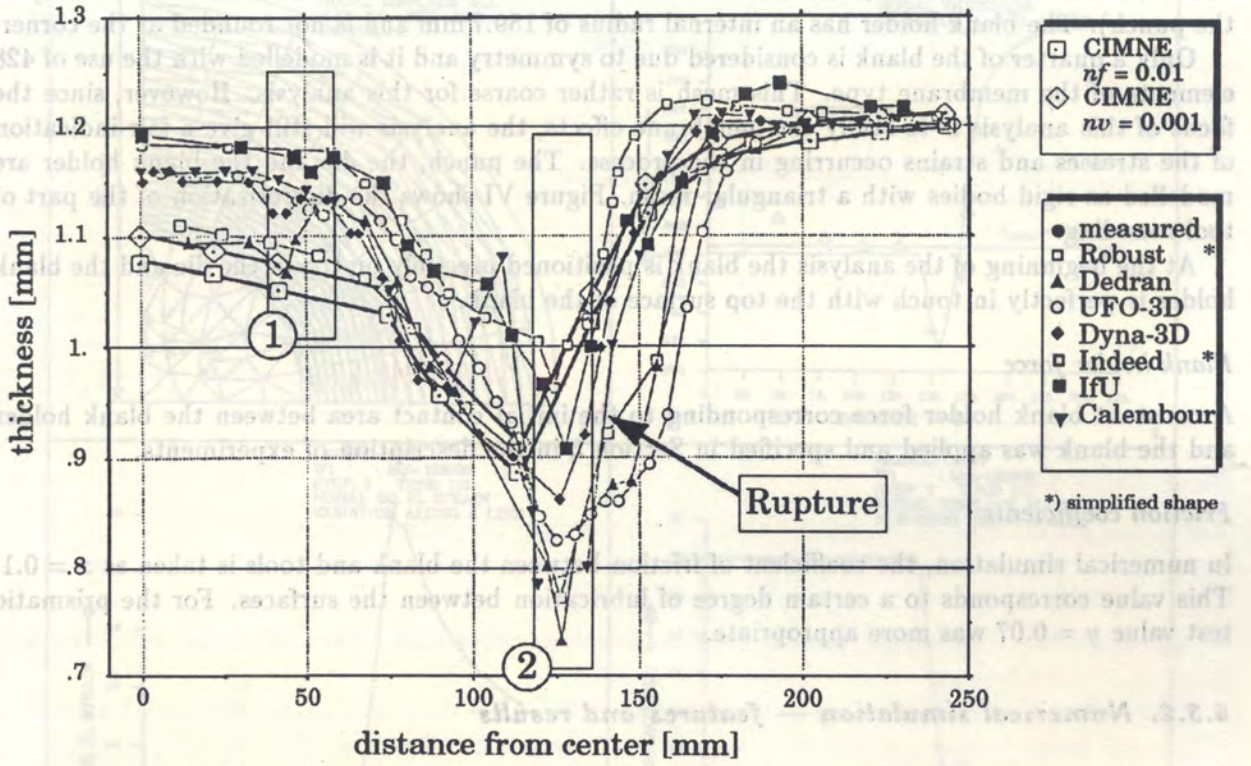

Fig. 12. VDI benchmark — thickness along line A as reported by different authors

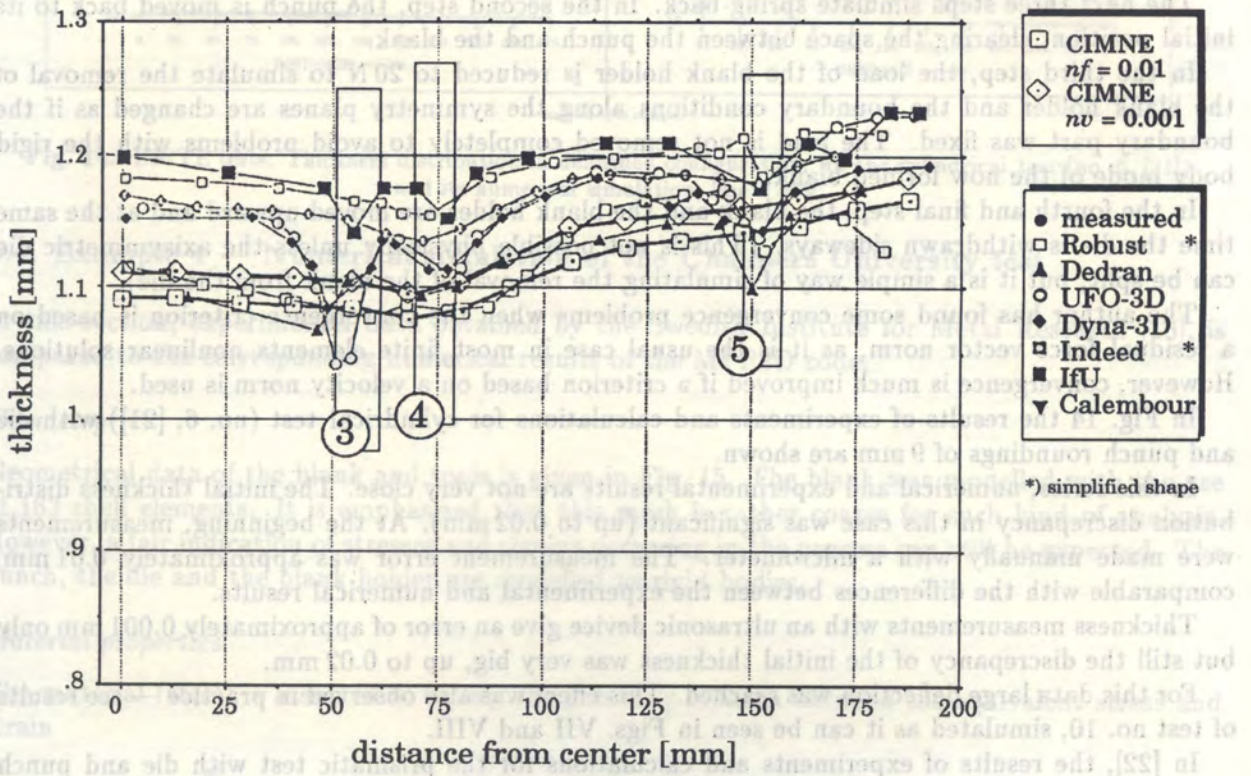

Fig. 13. VDI benchmark — thickness along line B as reported by different authors

The punch has a radius of 149.9 mm and is rounded at the corner with a radius of 9 mm. The die has an internal radius of 150.7 mm and is rounded at the corner with a radius of 9 mm (similarly as the punch). The blank holder has an internal radius of 159.7 mm and is not rounded at the corner.

Only a quarter of the blank is considered due to symmetry and it is modelled with the use of 428 elements of the membrane type. This mesh is rather coarse for this analysis. However, since the focus of this analysis is to study the membrane effects, the analysis will still give a fair indication of the stresses and strains occurring in the process. The punch, the die and the blank holder are modelled as rigid bodies with a triangular mesh. Figure VI shows the discretization of the part of tool rounding.

At the beginning of the analysis the blank is positioned precisely on top of the die and the blank holder is perfectly in touch with the top surface of the blank.

Blank holder force

A constant blank holder force corresponding to the initial contact area between the blank holder and the blank was applied and specified in Section 5 in the description of experiments.

Friction coefficients

In numerical simulation, the coefficient of friction between the blank and tools is taken as $x = 0.1$. This value corresponds to a certain degree of lubrication between the surfaces. For the prismatic test value $y = 0.07$ was more appropriate.

6.3.2. Numerical simulation — features and results

The entire numerical simulation is carried out in four steps. In the first step, the punch is moved down the whole distance obtained during experiment. This step models the actual drawing process.

The next three steps simulate spring-back. In the second step, the punch is moved back to its initial position, clearing the space between the punch and the blank.

In the third step, the load of the blank holder is reduced to 20 N to simulate the removal of the blank holder and the boundary conditions along the symmetry planes are changed as if the boundary part was fixed. The load is not removed completely to avoid problems with the rigid body mode of the now formed blank.

In the fourth and final step, the blank and the blank holder are moved upward and at the same time the die is withdrawn sideways. (This is not possible physically unless the axisymmetric die can be split, but it is a simple way of simulating the removal of the blank from the die).

The author has found some convergence problems when the convergence criterion is based on a residual force vector norm, as it is the usual case in most finite elements nonlinear solutions. However, convergence is much improved if a criterion based on a velocity norm is used.

In Fig. 14 the results of experiments and calculations for cylindrical test (no. 6, [21]) with die and punch roundings of 9 mm are shown.

In this series, numerical and experimental results are not very close. The initial thickness distribution discrepancy in this case was significant (up to 0.02 mm). At the beginning, measurements were made manually with a micrometer. The measurement error was approximately 0.01 mm, comparable with the differences between the experimental and numerical results.

Thickness measurements with an ultrasonic device give an error of approximately 0.001 mm only but still the discrepancy of the initial thickness was very big, up to 0.02 mm.

For this data large deflection was reached. This effect was also observed in practice — see results of test no. 10, simulated as it can be seen in Figs. VII and VIII.

In [22], the results of experiments and calculations for the prismatic test with die and punch roundings of 3, 6, and 9 mm are given. For small roundings only small deflection, up to 10 mm without oil (test no. 12, [22]) and up to 15 mm with oil (test no. 15, [22]) can be reached before collapse.

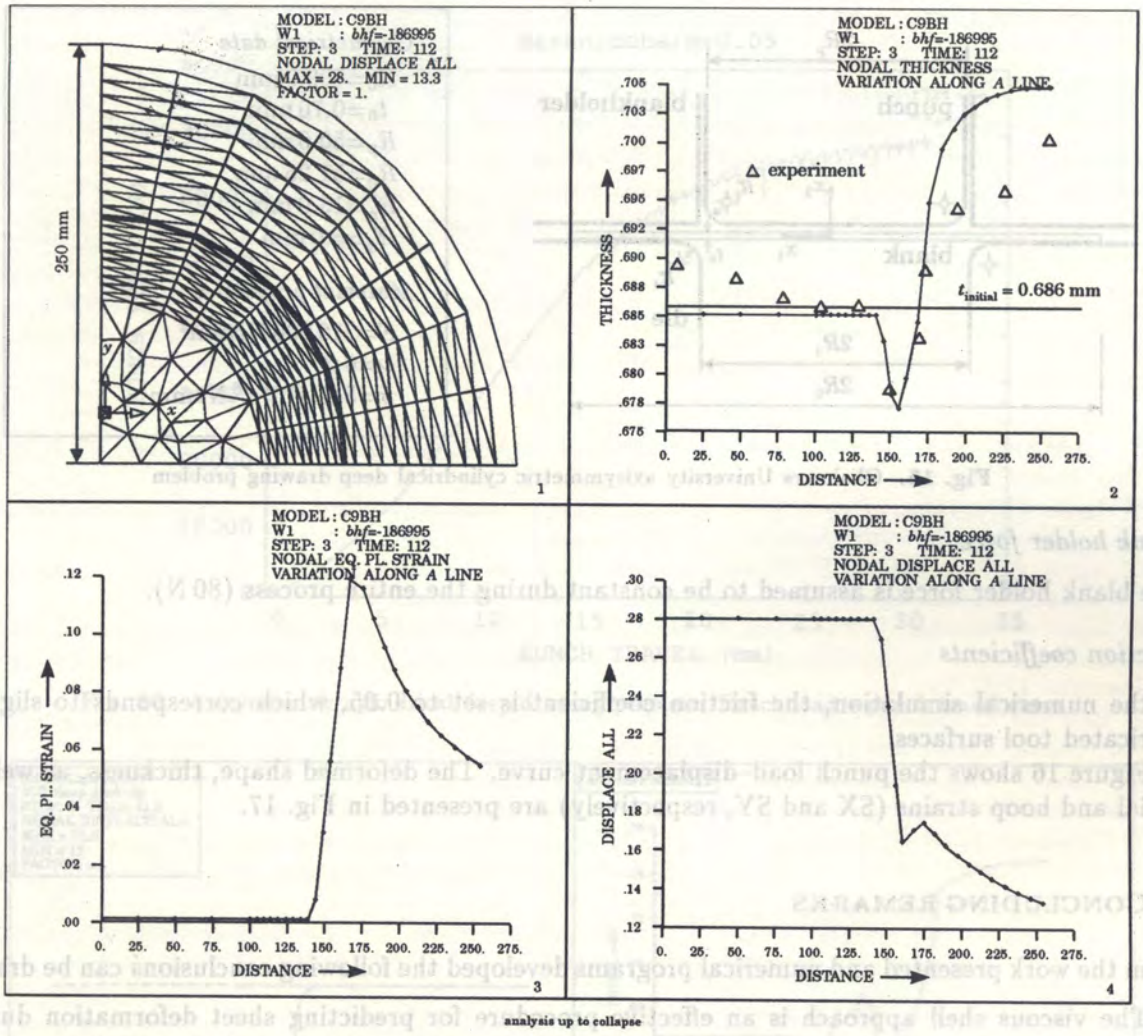

Fig. 14. BRITE tests. Thickness distribution in deformed configuration, for the cylindrical test (no. 6, [21]) and its numerical simulation, line $x = y$

6.4. Example 4 — Numerical simulation of the Chalmers University test

In this section, experimental data obtained by the Swedish Institute for Metal Research [15], is compared to the corresponding numerical results of the MFP2D code.

Geometry

Geometrical data of the blank and tools is given in Fig. 15. The blank was modelled with the use of 163 shell elements. It is emphasized that this mesh is rather coarse for such kind of analysis. However, a fair indication of stresses and strains occurring in the process can still be expected. The punch, the die and the blank holder are modelled as rigid bodies.

Material properties

The material (steel) is assumed to satisfy the following relation between the equivalent stress and strain

$$\bar{\sigma} = 547\bar{\varepsilon}^{0.18}\,\frac{\mathrm{N}}{\mathrm{mm}^2}\,. \tag{16}$$

The material is assumed to be isotropic.

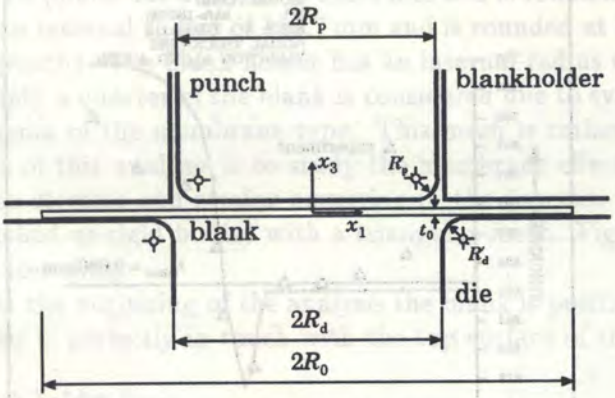

Geometrical data

R_0=100.0 mm
t_0=0.70 mm
R_p=50.0 mm
R_d=51.25 mm
R'_p=13.0 mm
R'_d=5.0 mm

Material properties

E=210 000 N/mm^2
ν=0.3
$\bar{\sigma}$=547$(\bar{\varepsilon}^p)^{0.18}$ N/mm^2

Fig. 15. Chalmers University axisymmetric cylindrical deep drawing problem

Blank holder force

The blank holder force is assumed to be constant during the entire process (80 N).

Friction coefficients

In the numerical simulation, the friction coefficient is set to 0.05, which corresponds to slightly lubricated tool surfaces.

Figure 16 shows the punch load–displacement curve. The deformed shape, thickness, as well as radial and hoop strains (SX and SY, respectively) are presented in Fig. 17.

7. Concluding Remarks

From the work presented and numerical programs developed the following conclusions can be drawn.

1. The viscous shell approach is an effective procedure for predicting sheet deformation during stamping operations. Both 2D and 3D formulations can be applied effectively to solve practical industrial problems.

2. The main drawback of this approach is its inability to predict elastic effects during spring-back operations. Future extensions of this procedure should go in that direction as well as towards the improvement of the computational efficiency of the codes developed.

3. The other drawback is the inability to deal with double contact problems typical of blank–rigid surfaces contact situations. Other models, like elasto-plastic solid or shell models, are more appropriate in this case.

4. Both drawbacks mentioned above can be overcome by approximate solutions proposed in this work. However, in this case many computational difficulties have to be faced. Some of them have been discussed and solved; others, for instance "artificial wrinkling" effects strongly coupled with contact and friction problems are still open for investigations.

5. Pre- and postprocessing have proved to be essential issues in the preparation of data and interpretation of results for the analysis of practical sheet stamping problems. The methodology developed as part of numerical applications to this work will certainly be of great use for future different codes for the numerical analysis of structures and process simulation.

6. The numerical codes have been validated with a number of numerical and experimental results. The experience gained in this work in the experimental testing of different sheet stamping problems will be essential for future validation of different computational models.

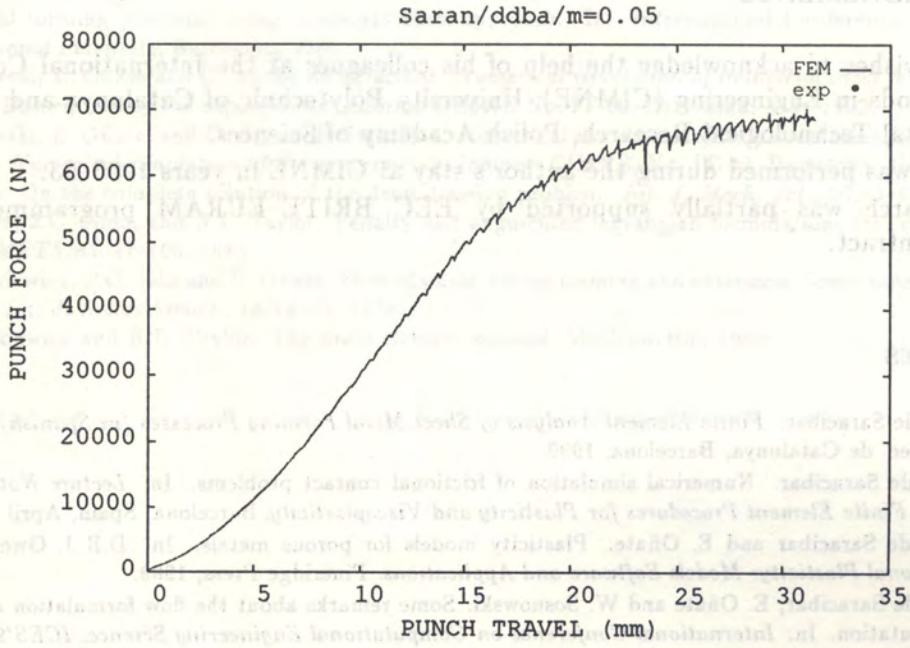

Fig. 16. Axisymmetric cylindrical deep drawing problem. Punch load – punch travel curve

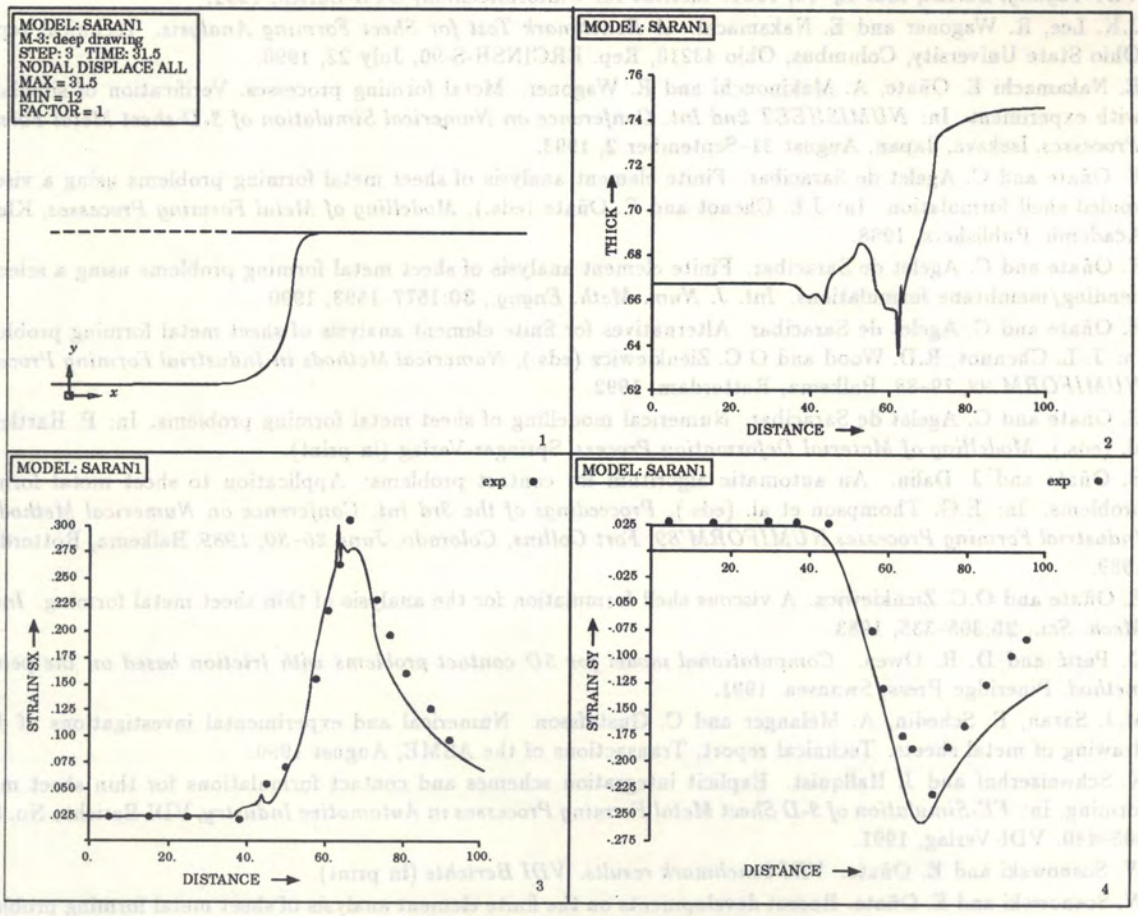

Fig. 17. Axisymmetric cylindrical deep drawing problem. The deformed shape and the distributions of thickness, radial strain (SX) and hoop strain (SY) for punch travel of 31.5 mm

ACKNOWLEDGEMENTS

The author wishes to acknowledge the help of his colleagues at the International Center for Numerical Methods in Engineering (CIMNE), University Polytechnic of Catalunya and the Institute of Fundamental Technological Research, Polish Academy of Sciences.

The work was performed during the author's stay at CIMNE in years 1990–93.

This research was partially supported by EEC BRITE–EURAM programme under the RI-1B-240 contract.

REFERENCES

[1] C. Agelet de Saracibar. *Finite Element Analysis of Sheet Metal Forming Processes (in Spanish).* Ph.D. Thesis. Univ. Politec. de Catalunya, Barcelona, 1990.

[2] C. Agelet de Saracibar. Numerical simulation of frictional contact problems. In: *Lecture Notes of the Short Course on Finite Element Procedures for Plasticity and Viscoplasticity*, Barcelona, Spain, April 2–3, 1992.

[3] C. Agelet de Saracibar and E. Oñate. Plasticity models for porous metals. In: D.R.J. Owen et al. (eds.), *Computational Plasticity: Models Software and Applications.* Pineridge Press, 1989.

[4] C. Agelet de Saracibar, E. Oñate and W. Sosnowski. Some remarks about the flow formulation and the spring-back computation. In: *International Conference on Computational Engineering Science, ICES'92*, Hong Kong, December 17–22, 1992.

[5] P. Hora and A. Krapoth. *FE-Simulation of 3-D Sheet Metal Forming Processes in the Automotive Industry. VDI-Tagung. Zürich, Mai 14–16, 1991.* Institut für Umformtechnik, ETH-Zürich, 1991.

[6] J.K. Lee, R. Wagoner and E. Nakamachi. *A Benchmark Test for Sheet Forming Analysis.* Technical report, Ohio State University, Columbus, Ohio 43210, Rep. ERCINSH-S-90, July 22, 1990.

[7] E. Nakamachi E. Oñate, A. Makinouchi and R. Wagoner. Metal forming processes. Verification of simulation with experiment. In: *NUMISHEET 2nd Int. Conference on Numerical Simulation of 3-D sheet Metal Forming Processes*, Isekava, Japan, August 31–September 2, 1993.

[8] E. Oñate and C. Agelet de Saracibar. Finite element analysis of sheet metal forming problems using a viscous voided shell formulation. In: J.L. Chenot and E. Oñate (eds.), *Modelling of Metal Forming Processes*, Kluwer Ačademic Publishers, 1988.

[9] E. Oñate and C. Agelet de Saracibar. Finite element analysis of sheet metal forming problems using a selective bending/membrane formulations. *Int. J. Num. Meth. Engng.*, **30**:1577–1593, 1990.

[10] E. Oñate and C. Agelet de Saracibar. Alternatives for finite element analysis of sheet metal forming problems, In: J.-L. Chennot, R.D. Wood and O.C. Zienkiewicz (eds.), *Numerical Methods in Industrial Forming Processes NUMIFORM 92*, 79–88. Balkema, Rotterdam, 1992.

[11] E. Oñate and C. Agelet de Saracibar. Numerical modelling of sheet metal forming problems. In: P. Hartley et al. (eds.), *Modelling of Material Deformation Process.* Springer-Verlag (in print).

[12] E. Oñate and J. Dalin. An automatic algorithm for contact problems: Application to sheet metal forming problems. In: E.G. Thompson et al. (eds.), *Proceedings of the 3rd Int. Conference on Numerical Methods in Industrial Forming Processes NUMIFORM'89, Fort Collins, Colorado, June 26–30, 1989.* Balkema, Rotterdam, 1989.

[13] E. Oñate and O.C. Zienkiewicz. A viscous shell formulation for the analysis of thin sheet metal forming. *Int. J. Mech. Sci.*, **25**:305–335, 1983.

[14] D. Perić and D. R. Owen. *Computational model for 3D contact problems with friction based on the penalty method.* Pineridge Press, Swansea, 1991.

[15] M.J. Saran, E. Schedin, A. Melanger and C. Gustafsson. Numerical and experimental investigations of deep drawing of metal sheets. Technical report, Transactions of the ASME, August 1990.

[16] K. Schweizerhof and J. Hallquist. Explicit integration schemes and contact formulations for thin sheet metal forming. In: *FE-Simulation of 3-D Sheet Metal Forming Processes in Automotive Industry,* VDI Berichte No. 894, 405–440. VDI-Verlag, 1991.

[17] W. Sosnowski and E. Oñate. *VDI benchmark results. VDI Berichte* (in print).

[18] W. Sosnowski and E. Oñate. Recent developments on the finite element analysis of sheet metal forming problems using a viscoplastic formulation. In: *FE-Simulation of 3-D Sheet Metal Forming Processes in Automotive Industry,* VDI Berichte No. 894, 307–323. VDI-Verlag, 1991.

[19] W. Sosnowski, E. Oñate and C. Agelet de Saracibar. Comparative study on sheet metal forming processes by numerical modelling and experiment. *Journal of Materials Processing Technology*, **34**:109–116, 1992.

[20] W. Sosnowski, E. Oñate and C. Agelet de Saracibar. Computational aspects in the finite element analysis of sheet metal forming problems using a viscous shell approach. In: *International Conference COMPLAS III, Computational Plasticity*, Barcelona, 1992.

[21] W. Sosnowski, E. Oñate and C. Agelet de Saracibar. *Numerical simulation of industrial sheet forming processes. Part I — Description of the experiments.* Informe CIMNE No. IT-60, Barcelona, May 1992.

[22] W. Sosnowski, E. Oñate, and C. Agelet de Saracibar. *Numerical simulation of industrial sheet forming processes. Part II — Numerical simulation of the experiments.* Informe CIMNE, No. IT-82, Barcelona, December 1992.

[23] D.M. Woo. On the complete solution of the deep drawing problem. *Int. J. Mech. Sci.*, **10**:83–94, 1968.

[24] P. Wriggers, J.C. Simo, and R.L. Taylor. Penalty and augmented lagrangian formulations for contact problems. *Proc. NUMETA'85*, 97–106, 1985.

[25] O.C. Zienkiewicz, P.C. Jain and E. Oñate. Flow of solids during forming and extrusion. Some aspects of numerical solutions. *Int. J. Solids Struct.*, **14**:14–28, 1978.

[26] O.C. Zienkiewicz and R.L. Taylor. *The finite element method.* McGraw-Hill, 1989.